HHS Public Access

Author manuscript

Langmuir. Author manuscript; available in PMC 2024 January 10.

Published in final edited form as:

Langmuir. 2023 January 10; 39(1): 295–307. doi:10.1021/acs.langmuir.2c02506.

Interactions of Bacterial Quorum Sensing Signals with Model Lipid Membranes: Influence of Membrane Composition on Membrane Remodeling

Curran G. Gahan[1], **Reid C. Van Lehn**[1], **Helen E. Blackwell**[2], **David M. Lynn**[1,2,*]

[1]Department of Chemical and Biological Engineering, University of Wisconsin–Madison, 1415 Engineering Dr., Madison, WI 53706, USA

[2]Department of Chemistry, University of Wisconsin–Madison, 1101 University Ave., Madison, WI 53706, USA

Abstract

We report the influence of membrane composition on the multi-scale remodeling of multicomponent lipid bilayers initiated by contact with the amphiphilic bacterial quorum sensing signal *N*-(3-oxo)-dodecanoyl-L-homoserine lactone (3-oxo-C12-AHL) and its anionic head group hydrolysis product, 3-oxo-C12-HS. We used fluorescence microscopy and quartz crystal microbalance with dissipation (QCM-D) to characterize membrane reformation that occurs when these amphiphiles are placed in contact with supported lipid bilayers (SLBs) composed of (i) 1,2-dioleoyl-sn-glycero-3-phosphocholine (DOPC) containing varying amounts of cholesterol, or (ii) mixtures of DOPC and either 1,2-dioleoyl-sn-glycero-3-phosphoethanolamine (DOPE; a conical zwitterionic lipid) or 1,2-dioleoyl-sn-glycero-3-phospho-L-serine (DOPS; a model anionic lipid). In general, we observe these mixed-lipid membranes to undergo remodeling events—including the formation and subsequent collapse of long tubules and the formation of hemispherical caps—upon introduction to biologically relevant concentrations of 3-oxo-C12-AHL and 3-oxo-C12-HS in ways that differ substantially from those observed in single-component DOPC membranes. These differences in bilayer reformation and their associated dynamics can be understood in terms of the influence of membrane composition on timescales of molecular flip-flop, lipid packing defects, and lipid phase segregation in these materials. The lipid components investigated here are representative of classes of lipids that comprise both naturally occurring cell membranes and many useful synthetic soft materials. These studies thus represent a first step toward understanding the ways in which membrane composition can impact interactions with this important class of bacterial signaling molecule.

Graphical Abstract

*(D.M.L.) dlynn@engr.wisc.edu.

Supporting Information. Additional plots and images providing qualitative and quantitative characterization and additional associated discussion of multicomponent bilayer remodeling promoted by bacterial amphiphiles (PDF). This material is available free of charge via the Internet.

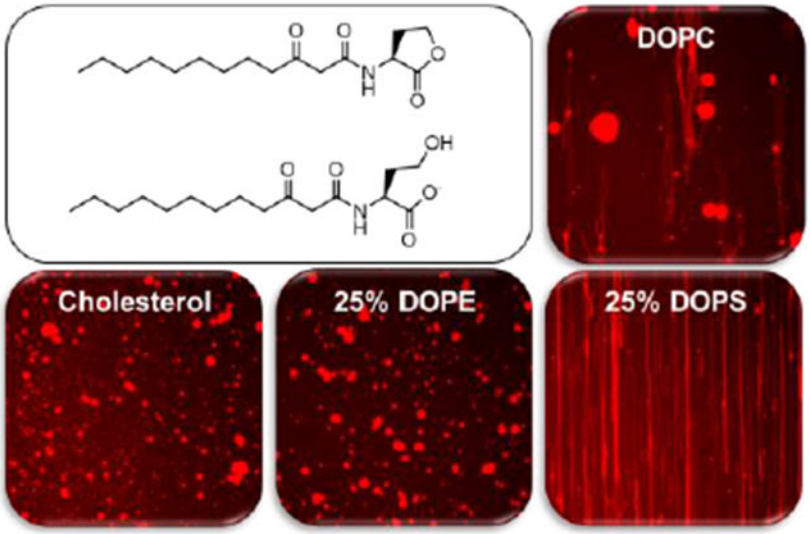

Introduction

The lipids that constitute the membranes of cells and many soft materials are structurally diverse and play major roles in facilitating cellular function and imparting other useful properties.[1–5] The membranes of mammalian cells comprise at least seven structurally unique types of lipids, including cholesterol, phosphatidylcholine (PC), phosphatidylethanolamine (PE), and phosphatidylserine (PS).[1,2] The relative compositions of these lipids influence many physical and mechanical properties of natural membranes, including surface charge, bending rigidity, and curvature.[6–9] Membrane composition also plays key roles in biological functions[1] such as protein binding specificity,[6] membrane fusion,[10] and cell division.[11] Most lipid-based assemblies are dynamic, and can undergo changes in physical properties, structural reformations, and molecular reorganization as a response to environmental stimuli, including changes in pH[3,12] and the presence of metal ions,[13–15] the adsorption of proteins,[16,17] or interactions with small molecules,[18–21] in ways that can depend critically on the relative abundance of each constituent lipid.

The work reported here was motivated broadly by recent studies by our group demonstrating that *N*-acyl L-homoserine lactones (AHLs), a class of nonionic, amphiphilic small-molecule signals used by common Gram-negative bacteria to coordinate collective behavior with cell density (i.e., quorum sensing),[22–24] can interact with and promote large-scale reformations in model, single-component lipid membranes composed of the phospholipid 1,2-dioleoyl-sn-glycero-3-phosphocholine (DOPC).[25,26] In this study, we sought to characterize interactions of AHLs with more complex, multi-component lipid membranes as a first step toward understanding how differences in membrane composition and properties (e.g., fluidity, etc.) can impact subsequent multi-scale remodeling in response to these bacterial signals.

AHLs possess a relatively polar homoserine lactone head group and an aliphatic tail of varying length (e.g., 3-oxo-C12-AHL, Figure 1),[22,23] and have previously been demonstrated to undergo molecular self-assembly in solution[27,28] and interact with other

self-assembled structures, including lipid bilayers,[25,26,29–32] in ways that are similar to other classes of non-ionic surfactants.[18–20,33] The homoserine lactone head group of AHLs is hydrolyzed in aqueous media (over hours to days, depending on tail structure), leading to anionic, ring-opened homoserine (HS) head group products[34,35] (e.g., 3-oxo-C12-HS, Figure 1) that have also been demonstrated to interact with lipid membranes.[25] Our group recently reported that 3-oxo-C12-AHL, 3-oxo-C12-HS, and other structurally related long-chained AHLs can interact with supported lipid bilayers (SLBs) composed of DOPC and promote the formation of extended micrometer-scale tubules and hemispherical 'caps' on the surfaces of the bilayers.[25,26] That past work also demonstrated that changes in the head and tail group structures of AHLs can impact the nature of these remodeling events substantially (e.g., leading to changes in the dynamics or relative proportions of these structures).[25,26] The results of those studies provide useful insight into fundamental factors, such as the timescales on which amphiphilic molecules translocate across lipid bilayers, that influence multi-scale remodeling and provide guidance for the design of synthetic materials that can respond to chemical products produced by bacterial communities. The single-component membrane models used in those studies do not, however, reflect the compositional complexities that are typical of many biological membranes (or many synthetic soft materials systems)[1–5] and that likely underlie many unexplored or currently unappreciated roles that AHLs (and their byproducts) could play in mediating interactions of bacteria with those systems. Of particular interest, in this context, are recent past studies demonstrating that lipid bilayers containing cholesterol or lipid rafts can interact with AHLs, and that these interactions can lead to subsequent membrane depolarization[29] to a greater extent than observed in membranes of reduced complexity or the mixing of segregated lipid phases.[32]

Here, we report on the influence of lipid membrane composition on multi-scale phenomena arising from interactions of model SLBs with 3-oxo-C12-AHL and its head group hydrolysis product, 3-oxo-C12-HS. We used fluorescence microscopy and quartz crystal microbalance with dissipation (QCM-D) to characterize multi-scale restructuring that occurs when these amphiphiles are placed in contact with SLBs comprising (i) DOPC containing varying amounts of cholesterol, or (ii) defined mixtures of DOPC and either 1,2-dioleoyl-sn-glycero-3-phosphoethanolamine (DOPE; a conical zwitterionic lipid) or 1,2-dioleoyl-sn-glycero-3-phospho-L-serine (DOPS; an anionic lipid) (see Figure 1). Each of these lipid components is representative of a class of lipids that are constituents of cell membranes;[2] these models thus represent a first, defined step toward understanding the ways in which membrane composition and structure can impact interactions with AHLs. In general, we observe these multicomponent membranes to undergo remodeling events upon introduction to biologically relevant concentrations of 3-oxo-C12-AHL and 3-oxo-C12-HS that differ from those observed in single-component DOPC membranes.[25] These observations likely reflect large differences in constituent lipid translocation timescales,[21,36] lipid packing,[6,37,38] lipid clustering,[15,39–41] and spontaneous curvature generation[15,42–44] in these mixed-lipid systems.

Overall, our results provide insight into the ways in which AHLs can interact with model lipid membranes of increasing complexity and provide additional support for the view that AHLs could potentially interact with more complex membranes of mammalian cells in

ways that extend beyond their currently understood roles in bacterial communication. As suggested above, the results of these studies also provide guidance that could be useful for the design of more sophisticated and compositionally complex soft materials (e.g., sensor elements or drug delivery vehicles) that respond selectively to molecules that mediate communication among bacteria in the mixed microbial environments in which they typically reside.

Materials and Methods

Materials.

1,2-Dioleoyl-sn-glycero-3-phosphoethanolamine (DOPE), chloroform, sodium chloride (NaCl), calcium chloride ($CaCl_2$) dimethylsulfoxide (DMSO), calcein, sodium hydroxide (NaOH), Sephadex G-50, triethylphosphine oxide, and deuterium oxide (D_2O) were obtained from Sigma (St. Louis, MO). 1,2-Dioleoyl-sn-glycero-3-phosphocholine (DOPC), 1,2-dioleoyl-sn-glycero-3-phospho-L-serine sodium salt (DOPS), 1,2-dioleoyl-sn-glycero-3-ethylphosphocholine chloride salt (DOEPC), 1,2-dihexanoyl-sn-glycero-3-phosphocholine (DHPC), filter supports, and a Mini-prep extruder were purchased from Avanti Polar Lipids (Alabaster, AL). Lissamine rhodamine B 1,2-dipalmitoyl-sn-glycero-3-phosphoethanolamine, triethylammonium salt (Rho-DPPE) was acquired from Invitrogen (Carlsbad, CA). Disposable culture tubes (16 × 100 mm) were purchased from VWR (West Chester, PA). Electrophoresis-grade sodium dodecyl sulfate (SDS) was obtained from Fisher Scientific (Pittsburgh, PA). Isopropanol (iPOH) was acquired from Fisher Scientific (Waltham, MA). Triton-X100 was obtained from Promega (Madison, WI). 3-(*N*-Morpholino)propanesulfonic acid (MOPS) was purchased from MP Biomedical (Irvine, CA). Minisort X plus 0.2 μm syringe filters were acquired from Sartorius Stedim Biotech (Goettingen, Germany). Polycarbonate extruder filters (100 nm) were purchased from Millipore (Billerica, MA). Deionization of distilled water was performed using a Milli-Q system (Millipore, Bedford, MA), with the resulting water with a resistivity of 18.2 MΩ. 3-oxo-C12-AHL and 3-oxo-C12-HS were synthesized according to previously reported methods.[25] All commercial materials were used as received without further purification unless otherwise specified. All experiments described to take place in buffer were in 150 mM NaCl, 10 mM MOPS, pH 7.4 solution. In some experiments, where noted, the buffer also contained 2 mM $CaCl_2$.

Preparation of AHL Solutions.

3-oxo-C12-AHL and 3-oxo-C12-HS stock solutions were prepared at a concentration of 20 mM in DMSO and stored at −4 °C. These stock solutions were thawed immediately before experiments were performed and diluted into DMSO to 100 times the final aqueous concentration. These DMSO solutions were then diluted 1:100 into buffer. To minimize changes in the ratios of hydrolyzed and unhydrolyzed AHL head groups in solution over time, all AHL solutions were used within 1 hour of initial dilutions of the DMSO stocks into buffer.

Optical Microscopy Experiments Using SLBs Formed by the Bicelle Fusion Method.

Fluorescence microscopy experiments were performed in Ibidi microfluidic chambers (μ-Slide VI 0.5 Glass Bottom) using fluorescently labeled SLBs (0.1 mol% Rho-DPPE) formed using a bicelle fusion method, as described in previous reports.[28,45–47] The microfluidic chambers were cleaned by incubating a 1 M NaOH solution in the cell for ~30 minutes prior to SLB formation and then washing with ample Milli-Q H_2O and then buffer. Briefly, solutions of the long-chained lipids (DOPC, cholesterol, DOEPC, DOPS, or DOPE) and the short-chained lipid DHPC in chloroform were mixed ([long chained lipid]/[DHPC] = 0.25), dried under a stream of dry N_2, and then placed under vacuum for at least an hour to remove any residual solvent. The lipid film was then hydrated by buffer or buffer containing 2 mM $CaCl_2$ to produce a 0.5 mM bicelle suspension, as determined by the total concentration of the long-chained lipid. This solution was then frozen and thawed five times by immersing the solution into an iPOH/dry ice bath and a warm water bath (~50 °C). After the samples were thawed in each cycle, they were vigorously vortexed. The bicelle stock solution was then diluted 1:16 or 1:32 for a final long-chained lipid concentration of 0.031 mM or 0.016 mM (depending on the lipids being used) and introduced to an Ibidi flow cell at a flow rate of 100 μL/min. The formation of a continuous bilayer was monitored by optical microscopy, and then buffer was introduced to the bilayer to wash away any remaining bicelles. Solutions of 3-oxo-C12-AHL or 3-oxo-C12-HS at various concentrations were introduced to the SLBs at a flow rate of 100 μL/min, and micrographs were acquired using an Olympus IX70 inverted microscope (Center Valley, PA) and a Q-imaging EXi Aqua camera (Tucson, AZ) every 5 seconds for ~8 minutes (at least 100 images). Fluorescently labeled lipids were excited with a Lumen Dynamics X-Cite Series 120PC-Q fiber coupled mercury lamp using the RFP channel (Monroe, LA). After the introduction of 3-oxo-C12-AHL or 3-oxo-C12-HS solutions to the bilayer, they were subsequently washed with the appropriate buffer at a flow rate of 100 μL/min to visualize changes in the bilayer structure when the test compounds were removed from solution.

Characterization Using Quartz Crystal Microbalance with Dissipation (QCM-D).

QCM-D measurements were performed using a Q-Sense E4 instrument (Bolin Scientific, Stockholm, Sweden) with QSensor QSX 303 quartz crystal sensors with a fundamental frequency of 5 MHz coated with 50 nm of SiO_2 (Bolin Scientific, Stockholm, Sweden). When received, the QCM-D sensors were cleaned as suggested by the manufacturer and as described previously.[25] Changes in frequency (ΔFrequency) and dissipation (ΔDissipation) as SLBs were formed or introduced to 3-oxo-C12-AHL or 3-oxo-C12-HS solutions were monitored at the third, fifth, seventh, ninth, and eleventh overtones and data analysis of multiple independent experiments was performed using the data from the seventh overtone. All graphs showing QCM-D data over time are the average frequency and dissipation changes over 60 second intervals of time. In all experiments, solutions were introduced to the quartz crystals at 100 μL/min using an Ismatic IPC High Precision Multichannel Dispenser peristaltic pump (Wertheim, Germany).

For QCM-D measurements, SLBs were formed using the bicelle fusion method as described above. Bicelle stock solutions in buffer (0.5 mM; as determined by long-chained lipid concentration) composed of DOPC or mixtures of DOPC and cholesterol, DOPE, DOPS,

or DOEPC were diluted to 0.031 mM or 0.16 mM in buffer and introduced to the sensor chamber. Adsorption of bicelles to the SiO_2 surface and subsequent fusion were monitored by QCM-D over time. The formed bilayer was then washed with buffer for at least 20 minutes. Solutions containing 3-oxo-C12-AHL or 3-oxo-C12-HS were then injected into the flow chamber and allowed to interact with the bilayer for 45 minutes. Subsequently, the bilayer was washed with buffer for an additional 45 minutes to observe the desorption of 3-oxo-C12-AHL or 3-oxo-C12-HS from the bilayer over time. Representative QCM-D traces for a single sensor are shown and discussed in the Supporting Information (Figures S1A, S3, S5, S7, and S11). Data analyses arising from these QCM-D experiments presented in all other Figures are from 3 or 4 (n = 3–4) independent experiments run simultaneously on different crystals. Statistical significance was determined using Student's t-test. During experiments, the measurement chamber was held at 25 ± 0.5 °C. Immediately following each experiment, the quartz crystal resonators were washed according to the manufacturer's instructions and described previously before storage between measurements.[25]

Preparation of Calcein-Loaded Vesicles.

Large unilamellar vesicles (LUVs) containing different amounts of cholesterol and loaded with calcein were prepared using a freeze-thaw and vesicle extrusion procedure as described previously.[25] In brief, desired amounts and compositions of lipids dissolved in chloroform were aliquoted into vials and the chloroform was removed under a stream of dry nitrogen and further dried under vacuum for at least an hour. The dried lipid film was then hydrated with a 70 mM calcein solution in buffer (pH = 7.4) and vortexed vigorously to form a turbid 5 mg/mL suspension of multilamellar vesicles. The resulting vesicle suspension was then frozen and thawed five times by sequential immersion in an iPOH/dry ice bath and a warm water bath (~50 °C) and vortexed vigorously, and then passed at least 11 times through a 100 nm PC filter using an Avanti Polar Lipids Mini-prep extruder to produce unilamellar vesicles. After extrusion, the resulting vesicles were washed and separated from residual external calcein using a hand-packed Sephadex G-50 chromatography column. ^{31}P NMR was used as described in the Supporting Information to quantify the concentration of the resulting purified vesicle solution.

Calcein leakage assays were performed as previously described using a Tecan Infinite 200 Pro plate reader.[25,26] In these assays, the vesicle suspensions were diluted 10x into AHL-containing solutions and allowed to sit for at least five minutes. All tests were repeated three times (n = 3) for each batch of vesicles and were performed with three (n = 3) independently produced batches of vesicles for a total of nine (n = 9) fluorescence measurements. Statistical significance against the buffer control was determined using a one-way ANOVA with all nine normalized replicates for each condition used that was corrected for multiple comparisons using Dunnett's method. The fluorescence intensity for each reading was normalized as described in Equation 1 where: FI is the fluorescence intensity of the test solution, FI_{Buffer} is the fluorescence intensity of the calcein vesicles in buffer as the negative control, and $FI_{TX\text{-}100}$ was the fluorescence intensity of a vesicle solution containing 1% Triton X-100 (which is known to lyse vesicles[48]) as a positive control.

$$Normalized\ Flourescense = \frac{FI - FI_{Buffer}}{FI_{TX-100} - FI_{Buffer}} \quad \text{(Eq. 1)}$$

Results and Discussion

We recently reported on the influence of AHL head[25] and tail[26] group structure on membrane remodeling in single-component SLBs of DOPC formed using either a vesicle fusion[25] or bicelle formation[26] technique. Other groups have reported that it can be difficult to form some compositionally complex, mixed-lipid SLBs using the vesicle fusion technique[46,49] and that even single-component bilayers are often non-homogeneous and can contain unruptured vesicles that appear as optical defects.[50] Recent reports by Cho and coworkers demonstrate that more uniform SLBs containing assorted glycerophospholipids and relatively high amounts of cholesterol can be formed on metal oxide substrates using the bicelle formation technique.[45,46] For the studies described here, we used the bicelle formation technique to produce SLBs composed of either (i) DOPC alone or (ii) multicomponent bilayers composed of mixtures of DOPC with defined amounts of cholesterol, DOPS, or DOPE (Figure 1). We selected this subset of lipids because they are representative of classes of lipids naturally present in the membranes of mammalian cells and have a variety of impacts on the physicochemical properties of lipid bilayers, including differences in surface charge, lipid packing, and curvature.[2,6,43,44] Additionally, all of these lipids possess two oleic acid tails, and bilayer membranes formed from them are, thus, fluid at room temperature.[51] The studies below were performed using 3-oxo-C12-AHL or 3-oxo-C12-HS to permit characterization of the influence of AHL head group structure (Figure 1) on membrane association and remodeling. 3-oxo-C12-AHL is an important quorum sensing (QS) signal molecule used by the bacterial pathogen *Pseudomonas aeruginosa*,[52] and thus has relevance to understanding a range of bacterial behaviors that have broad health care and commercial impacts.[53–57]

We began our studies by characterizing and validating the formation of DOPC SLBs containing 10 mol% or 30 mol% cholesterol on SiO_2-coated quartz crystals and NaOH-treated glass slides used in the QCM-D and fluorescence microscopy experiments described in sections below. Using QCM-D, we observed changes in frequency of ~25 Hz and changes in dissipation of less than 0.5 $x10^{-6}$ (as compared to bare SiO_2 crystals; Figure S1), consistent with past studies and suggesting the formation of continuous SLBs.[46] As shown in Figure S2, characterization by fluorescence microscopy revealed SLBs containing 10 mol% cholesterol to be continuous and largely devoid of optical defects (Figure S2B). However, we observed variation in the optical quality of SLBs containing 30 mol% cholesterol; these bilayers sometimes appeared non-homogeneous, with areas of the bilayer having significant optical defects (Figure S2C), and were sometimes observed to be more uniform (Figure S2D). We note that Cho and coworkers determined that 30 mol% cholesterol is the highest cholesterol content that could be consistently incorporated into SLBs using the bicelle formation technique, which could, in part, account for the inhomogeneities observed here.[46]

As part of these initial studies, we also formed bilayers composed of mixtures of 75% DOPC and 25% of either (i) DOPE or (ii) DOPS by adapting previously described procedures.[45,47] For the formation of bilayers containing the zwitterionic lipid DOPE, we found bilayer formation to be more consistent when we used a lower concentration of bicelle solution (0.015 mM vs. 0.031 mM by total long tailed lipid concentration) than was reported to be optimal for the formation of SLBs in past studies using the bicelle method.[45,47] The DOPE-containing bilayers formed using this approach registered frequency and dissipation shifts of −26.2 ± 0.7 Hz and 0.6 ± 0.05 x10^{-6}, respectively, compared to a bare SiO_2 quartz crystal (Figure S1). Characterization by optical microscopy revealed non-homogeneous structures with some regions containing continuous bilayers with a relatively low number of optical defects (e.g., Figure S2E) and other areas containing structures that protruded from the bilayer surface (e.g., Figure S2F). These latter structures could result from the negative spontaneous curvature of DOPE lipids[43,44] and their resulting behaviors during the formation of these low-curvature SLBs. All microscopy observations described below on SLBs of this mixed DOPC/DOPE system were made in regions containing continuous areas of the bilayer.

The formation of DOPC SLBs containing 25 mol% DOPS on SiO_2 surfaces proved more challenging in the simple buffer solutions used to form the SLBs above, likely because interactions of anionic bicelles with SiO_2 surfaces are unfavorable due to charge repulsion.[45] We therefore formed our DOPS-containing SLBs using buffer containing 2 mM $CaCl_2$, as divalent calcium ions can associate with the anionic serine head groups in DOPS and promote adsorption and fusion of the bicelles on the SiO_2 surface.[58] Under these conditions, we observed changes in frequency and dissipation of −25.4 ± 0.8 Hz and 0.2 ± 0.2 x10^{-6} (Figure S1), respectively, and the formation of homogeneous bilayers relatively devoid of optical defects by fluorescence microscopy (Figure S2H). We note here that addition of Ca^{2+} during bilayer formation can lead to changes in the physical properties of anionic bilayers, including the formation of DOPS-rich domains,[15,39–41] the formation of bilayer curvature,[15,42] increased lipid packing density,[59,60] partial bilayer dehydration,[41,61,62] and decreased membrane fluidity.[60] To understand some of the potential impacts of Ca^{2+} in these DOPC/DOPS mixed-lipid SLBs, we also characterized the properties of single-component DOPC SLBs formed in the presence of Ca^{2+} (Figure S1, Figure S2G). We return to a discussion of the potential impacts of Ca^{2+} in these SLBs again in the sections below.

Interactions of 3-oxo-C12-AHL with DOPC Membranes Containing Cholesterol

In a first series of QCM-D studies, we introduced solutions of 3-oxo-C12-AHL to DOPC SLBs containing 10 mol% or 30 mol% cholesterol formed on SiO_2-coated quartz crystal sensors and compared these to single-component DOPC SLBs (i.e., 0% cholesterol). We selected these cholesterol compositions because 30 mol% cholesterol is at the upper end of the range that can be incorporated into SLBs using the bicelle formation method, and compositions at 10 mol% allowed us to probe the contribution of cholesterol to 3-oxo-C12-AHL induced bilayer reformation at a second, intermediate concentration.[46] Introduction of a 50 μM solution of 3-oxo-C12-AHL to single-component DOPC bilayers yielded changes of frequency and dissipation of −4.0 ± 1.0 Hz and 1.5 ± 0.1 x10^{-6}, respectively (see Figure 2) for analyses of bilayer reformation from multiple trials after 45 minutes of exposure

to 3-oxo-C12-AHL and Figure S3A for representative time course data). We note that 50 μM is well within the range of concentrations of AHLs estimated within bacterial biofilms[63] and is comparable to AHL concentrations reported to be present in some quorate bacterial cultures.[64] These results are generally consistent with the changes of frequency and dissipation measured upon exposure of DOPC bilayers to solutions of 3-oxo-C12-AHL at 50 μM in our past studies.[25,26] However, when cholesterol was incorporated into the bilayer, we observed smaller changes in both frequency and dissipation upon exposure to 50 μM 3-oxo-C12-AHL solutions, with changes of (-2.7 ± 0.2 Hz and $0.9 \pm 0.3 \times 10^{-6}$) and ($-2.0 \pm 0.3$ Hz and $0.8 \pm 0.2 \times 10^{-6}$) for SLBs containing 10 mol% and 30 mol% cholesterol, respectively (Figure 2 and Figure S3(B–C)). These smaller changes in frequency and dissipation at higher cholesterol composition were surprising, as previous reports suggested that AHLs had a higher binding capacity to[29] and preferentially interacted with[32] cholesterol containing bilayers, but we note that our results exhibit trends similar to those reported previously for measurements of cholesterol-containing SLBs exposed to other non-ionic amphiphiles.[46] These differences in frequency and dissipation shifts can be understood in terms of the ability of cholesterol to quickly flip-flop across a bilayer to decrease asymmetrical bilayer stresses (*vide infra*).[21]

We observed large and visually apparent changes in membrane reformation when otherwise identical experiments were characterized by fluorescence microscopy. The addition of 50 μM solutions of 3-oxo-12-AHL to single-component DOPC SLBs initiated the formation of short tubules, some of which subsequently collapsed into hemispherical caps on the surface of the bilayers (see Figure 3A for microscopy images after 360 sec of exposure to 3-oxo-C12-AHL and Figure S4A for microscopy images at other selected time points). At higher concentrations of 3-oxo-C12-AHL (200 μM; above the previously reported critical aggregation concentration of this AHL in solution[28]), we observed the formation of extended tubule structures hundreds of microns in length; some of these extended tubules collapsed into larger hemispherical caps over time, while others remained on the surface of the bilayer over the duration of the experiment (360 sec; see Figures 3D and S4B). Overall, these results are broadly consistent with those of our past studies on the interactions of 3-oxo-C12-AHL with this single-component DOPC system.[25,26] We note again that 200 μM is above the critical aggregation concentration of 3-oxo-C12-AHL;[28] it is therefore possible that differences in interactions observed at this higher concentration could also result, at least in part, from the presence AHL aggregates and the interactions of those aggregates with lipid membranes, as observed in our previous study.[25] In contrast, we observed differences in behavior when 3-oxo-C12-AHL was added to SLBs containing cholesterol. As shown in Figure 3(B–C) and Figure S4A, introduction of 50 μM 3-oxo-C12-AHL to bilayers containing cholesterol also resulted in the formation of tubules on the surface of the bilayer, but these tubules were shorter and thinner and collapsed or retracted more quickly into hemispherical caps as compared to bilayers that did not contain cholesterol. Similar structures and dynamics were observed when a 200 μM solution of 3-oxo-C12-AHL was introduced to the bilayers (Figure 3(E–F), Figure S4B). We note that the final sizes of the hemispherical caps observed in these experiments (e.g., after 360 sec) were generally observed to decrease with increasing cholesterol composition.

As mentioned above, differences in the membrane remodeling observed here upon the addition of 3-oxo-C12-AHL to bilayers of varying cholesterol composition likely result from the fast timescales over which cholesterol is able to flip-flop across a bilayer to relieve asymmetrical bilayer stresses.[36,65] As reported in our past studies, the formation of tubules upon the introduction of an amphiphile to an SLB, and the time-dependent retraction of these features into hemispherical caps, can be understood, at least in part, in terms of the accumulation and subsequent relief of asymmetrical stresses between the leaflets of the bilayer (with a relief of stress leading to a transition from high curvature tubules to lower curvature hemispherical caps).[25,26] In a cholesterol-free bilayer, this transition would likely be dominated by the timescale on which flip-flop of the interacting amphiphilic species occurs (we note that phospholipid flip-flop typically occurs on timescales that are much slower than those of single-tailed amphiphiles).[36] For cholesterol-containing bilayers, however, these stresses can also be relieved by the flip-flip of cholesterol across the bilayer.[36] Because flip-flip of cholesterol can occur on relatively fast timescales, we would anticipate (and do observe) transitions from tubules to hemispherical caps to occur more rapidly. Additionally, the negative spontaneous curvature of cholesterol[43] could additionally play a role in the formation of low curvature hemispherical caps as opposed to high curvature extended tubule structures when placed in contact with 3-oxo-C12-AHL, as the spontaneous curvature of surfactants has been described to change the bilayer restructuring observed.[66] Taken together, the results of our optical microscopy and QCM-D experiments reveal that cholesterol can play a significant role in modulating the interactions of lipid bilayers with 3-oxo-C12-AHL and provide insight into the ways in which timescales of lipid flip-flip can influence interactions with AHLs and subsequent multi-scale responses.

Lastly, we note that 3-oxo-C12-AHL has also been demonstrated to promote tubule formation in the (unsupported) lipid membranes of GUVs and that treatment of large unilamellar vesicles (LUVs) composed of DOPC with this AHL can lead to low, but statistically significant, levels of leakage of the fluorescent dye calcein encapsulated in the vesicles.[25,26] We performed a series of experiments to characterize the impact of cholesterol on dye leakage in DOPC LUVs containing 10 mol% and 30 mol% cholesterol. As shown in Figure 4, we observed low levels of calcein leakage in these cholesterol-containing lipid vesicles, corresponding to 5.18 ± 0.77 % and 4.74 ± 1.51% leakage at a concentration of 180 μM 3-oxo-C12-AHL in 10 mol% (Figure 4A) and 30 mol% (Figure 4B) cholesterol vesicles, respectively. These levels of dye leakage are similar to those reported previously for DOPC vesicles (~5% leakage at 180 μM), suggesting that the presence of cholesterol does not affect vesicle leakage substantially. This result was, to some extent, unexpected, as cholesterol has been previously proposed to increase the stability of vesicles in the presence of single-tailed amphiphiles.[18,67] We note that previous reports have correlated membrane permeabilization to the accumulation of surfactants, and by extension stress, in the outer leaflet of the bilayer.[18,68,69] While cholesterol is able to readily alleviate asymmetrical bilayer stresses, it may occur on timescales slower than those required to cause leakage, as suggested by the formation of small tubules on the surface of the SLBs. The leakage observed here could therefore occur due to the accumulation of stresses in the bilayer or through a different mechanism.

Interactions of 3-oxo-C12-AHL and 3-oxo-C12-HS with Bilayers Containing DOPE

We performed an additional series of studies to characterize the interactions of 3-oxo-C12-AHL with SLBs of DOPC containing DOPE. In contrast to DOPC, DOPE is a conical shaped zwitterionic lipid with negative spontaneous curvature (Figure 1),[43,44] and can promote lipid packing defects when incorporated into bilayers with cylindrical lipids.[6,37] For these studies, we also included 3-oxo-12-HS, the anionic head group hydrolysis product of 3-oxo-C12-AHL, in order to characterize the influence of AHL head group structure on multi-scale phenomena in this mixed-lipid system.

As shown in Figure 5 and Figure S5(C–D), the introduction of 50 μM solutions of 3-oxo-C12-AHL and 3-oxo-C12-HS to SLBs containing 75% DOPC and 25% DOPE on SiO_2-coated quartz crystal sensors resulted in changes in dissipation and frequency of (-3.2 ± 1.0 Hz and 1.1 ± 0.2 x10^{-6}) and (-1.4 ± 0.1 Hz and 0.5 ± 0.1 x10^{-6}), respectively. These changes in frequency and dissipation for 3-oxo-C12-HS solutions are similar to those of DOPC bilayers introduced to this compound under otherwise identical conditions; in contrast, the change in dissipation observed for 3-oxo-C12-AHL solutions is lower in DOPE containing bilayers than those previously observed in DOPC bilayers (Figure 5). Analogous fluorescence microscopy experiments to characterize interactions of 3-oxo-C12-AHL (Figure 6B and Figure S6C) with these DOPE-containing bilayers revealed the immediate and apparently direct formation of hemispherical caps on the surfaces of the bilayers (that is, we did not observe these caps to form by the initial formation and subsequent retraction of extended tubule structures). The introduction of 3-oxo-C12-HS at a concentration of 50 μM (Figure 6F and Figure S6C) appeared to lead to the formation of hemispherical caps that appeared to be more protruded from the surface of the bilayer than those reported in our previous studies.[25,26,70] Additional studies will be required to investigate possible differences in these structures more completely.

In contrast to the results at 50 μM, 3-oxo-C12-AHL formed very short tubules (~10 μm in length) at 200 μM that collapsed, over approximately the first minute of the experiment, into small hemispherical caps that subsequently grew in size over the remaining five minutes of the experiment (Figure 6D and Figure S6D). Overall, the sizes of the hemispherical caps in these mixed-lipid bilayers remained smaller than the caps observed to form in single-component DOPC bilayers under otherwise identical conditions (Figure 6C and Figure S6B). At this higher 200 μM concentration, 3-oxo-C12-HS initiated the formation of predominantly short (~10 μm) tubules and some hemispherical caps that extended from the surface of the bilayer (as described above), both of which persisted for the duration of the experiment (Figure 6H and Figure S6D).

The differences in membrane restructuring observed upon the addition of these amphiphiles to DOPE-containing bilayers, relative to those observed in single-component DOPC bilayers, likely arise, at least for 3-oxo-C12-AHL, from lipid packing defects in these mixed-lipid SLBs.[71] As noted above, it is well known that the mixing of conical lipids and cylindrical lipids, especially those with unsaturated aliphatic tails, as used here, can lead to the formation of packing defects.[6,37] Similar deviations from ideal packing in DSPE-DSPC mixtures have been demonstrated to decrease the timescales on which the lipids that compose those membranes are able to flip-flop across the bilayer.[38,72] Our past

studies on the interactions of AHLs with lipid bilayers, and those of other groups using other synthetic amphiphiles, provide a framework for understanding the formation and associated dynamics of tubules and hemispherical caps in terms of the timescales over which an adsorbed or intercalated amphiphile is able to translocate across the bilayer (i.e., from the outer leaflet to the inner leaflet) to relieve asymmetrical bilayer stresses.[25,26] If the presence of lipid packing defects in these DOPE-containing bilayers were able to also increase rates of AHL translocation, this general framework would suggest the possibility that tubules (which are high-curvature structures formed by the initial accumulation of amphiphile in the outer leaflet of the membrane) would transition more rapidly to hemispherical caps (which are lower-curvature structures that result from flip-flop and relief of asymmetrical stress) than they do in bilayers that do not contain such packing defects. The results reported here are consistent with this possibility, as we generally observe faster transitions from tubules to caps in our 3-oxo-C12-AHL experiments with mixed DOPC/DOPE bilayers, as compared to otherwise identical DOPC bilayers. Additional experiments will be required to understand the interactions of these mixed-lipid membranes with 3-oxo-C12-HS. We note that our results do not preclude differences in bilayer reformations observed for both 3-oxo-C12-AHL and 3-oxo-C12-HS to potentially result from the negative spontaneous curvature of DOPE, a factor that has previously been suggested to alter the interactions of lipids and surfactants as suggested above.[66] Additionally, the results of these current experiments do not permit meaningful conclusions about the extent to which packing defects might affect differential rates of translocation of 3-oxo-C12-AHL and 3-oxo-C12-HS across the bilayer.

In a broader context, we note that while the DOPE-containing mixed-lipid system used here is compositionally more complex than the single-component DOPC membranes used in our past studies,[25,26] it is substantially less complex than lipid membranes in bacterial or mammalian cells.[2] However, packing defects characterized in this mixed-lipid system can serve as models to probe and understand the roles that lipid packing defects and other associated phenomena may play in the transport of agents across cell membranes or other synthetic lipid bilayers comprised of mixtures of cylindrical and conical lipids. The results of these current studies may thus provide useful insight into the roles that lipid packing defects could play in facilitating the translocation of AHLs across these more complex membranes.

Interactions of 3-oxo-C12-AHL and 3-oxo-C12-HS with Charged Bilayers

We conducted a final series of experiments to characterize the interactions of 3-oxo-C12-AHL and 3-oxo-C12-HS with DOPC SLBs containing charged lipids. For these studies, we selected the naturally occurring anionic lipid DOPS (Figure 1) as a model. We note again here that all DOPS-containing SLBs used in experiments described below were formed using the bicelle formation method in buffer containing 2 mM $CaCl_2$ to facilitate the formation of uniform SLBs on anionic SiO_2 surfaces (see Methods for additional details). It has been previously suggested that Ca^{2+} can strongly bind to zwitterionic and anionic bilayers and change the physical properties of both. For example, the addition of Ca^{2+} to single-component DOPC bilayers can decrease the area per lipid molecule,[73] increase membrane thickness,[73,74] and, at high concentrations, decrease membrane fluidity.[75] In

addition to the effects listed above,[41,59–62] in anionic bilayers, the addition of Ca^{2+} can lead to the formation of anionic lipid domains[15,39–41] that can introduce curvature into charged bilayers.[15,42]

To facilitate more direct comparisons between single-component DOPC and multicomponent DOPC/DOPS bilayers formed in the presence of Ca^{2+}, we first characterized bilayer remodeling in DOPC bilayers in the presence of buffer containing 2 mM $CaCl_2$. As shown in Figures 7 and S7(A,B), introduction of 50 μM solutions of 3-oxo-C12-AHL and 3-oxo-C12-HS to DOPC bilayers in the presence of Ca^{2+} resulted in changes in frequency and dissipation of (-4.1 ± 0.9 Hz and $1.0 \pm 0.1 \times 10^{-6}$) and ($-0.1 \pm 0.1$ Hz and $0.2 \pm 0.02 \times 10^{-6}$), respectively. We note that the introduction of calcium to the buffer solution led to small but statistically significant differences in dissipation change upon the introduction of 3-oxo-C12-AHL to the bilayers ($p<0.005$; compared to DOPC bilayers in buffer not containing 2 mM $CaCl_2$). This difference in dissipation change suggests differences in the re-structuring that is occurring on the surface of the bilayer (*vide infra*). The changes in frequency and dissipation observed upon the introduction of 3-oxo-C12-HS to the bilayer in the presence of Ca^{2+} were statistically similar to those observed in the absence of Ca^{2+} under otherwise identical conditions.

Fluorescence micrographs shown in Figures 8(A,C,E,G) and S8(A,B) show that the introduction of non-ionic 3-oxo-C12-AHL to DOPC bilayers in buffer containing $CaCl_2$ at 50 μM or 200 μM led to the formation of tubules that were shorter and that collapsed more quickly into hemispherical caps than observed in DOPC bilayers in the absence of $CaCl_2$, which could play a role in the differences in dissipation observed in our QCM-D experiments. In contrast, introduction of anionic 3-oxo-C12-HS at 50 μM led to no observable membrane restructuring. At higher concentrations of 200 μM, the introduction of 3-oxo-C12-HS led to the formation of hemispherical caps within the first 30 seconds of the experiment and qualitatively less bilayer reformation than that observed in otherwise identical DOPC bilayers in the absence of Ca^{2+}. Taken together, these results demonstrate that the presence of Ca^{2+} leads to changes in the multi-scale remodeling that occurs when these compounds interact with DOPC membranes. It is likely that these changes result from one or more of the impacts of Ca^{2+} on membrane properties discussed above (e.g., decreased membrane fluidity, bilayer thickening, or bilayer compression, etc.)[73–75] and their resulting impacts on the intercalation and subsequent translocation of 3-oxo-C12-AHL or 3-oxo-C12-HS. We note, in this latter context, that it is also possible that, in experiments using 3-oxo-C12-HS, Ca^{2+} ions could also coordinate to the anionic head group and form dimers in solution, thereby changing the solution phase behavior of this compound or, by extension, its interactions with bilayers. We return to this possibility again in the discussion below.

QCM-D experiments in which 3-oxo-C12-AHL and 3-oxo-C12-HS were introduced, at concentrations of 50 μM, to SLBs containing 75 mol% DOPC and 25 mol% DOPS resulted in changes in frequency and dissipation of (-1.4 ± 0.5 Hz and $1.1 \pm 0.1 \times 10^{-6}$) and ($-2.3 \pm 0.5$ Hz and $0.8 \pm 0.2 \times 10^{-6}$), respectively [Figures 7 and S7(C–D)]. This result was surprising, because it suggests that, when compared to the DOPC bilayers in the presence of Ca^{2+} discussed above, less 3-oxo-C12-AHL associates with the bilayer (smaller changes

in frequency), but that this leads to otherwise similar amounts of membrane restructuring (similar changes in dissipation). In our past experiments and the results described above, increases in dissipation are generally accompanied by increases in frequency.[25,26] The results shown in Figure 7 thus hint at the possibility of significant changes in the structures or dynamics of features observed that could occur on the surfaces of these DOPS-containing bilayers (*vide infra*). In contrast, the introduction of 3-oxo-C12-HS to DOPS-containing bilayers resulted in larger changes in frequency and dissipation relative to those observed in single-component DOPC bilayers under otherwise identical conditions. Although the reasons for this are not completely understood, it is possible that increased adsorption or intercalation of this anionic compound to the anionic DOPS component lipids in these mixed bilayers could be facilitated either by (i) the chelation-induced dimerization of 3-oxo-C12-HS by Ca^{2+} ions in solution or (ii) the chelation-induced association of 3-oxo-C12-HS with the serine head group of DOPS on the surface of the bilayer, as also discussed above.[41]

Characterization of interactions of 3-oxo-C12-AHL and 3-oxo-C12-HS with DOPS-containing SLBs by fluorescence microscopy revealed large differences in bilayer remodeling compared to otherwise identical DOPC bilayers. As shown in Figure 8(F,H) and Figure S8(C,D), the introduction of solutions containing 3-oxo-C12-HS to DOPS-containing bilayers led to substantially more membrane reformation than we observed in single-component DOPC bilayers (Figure 8(E,G)), with the formation of hemispherical caps (at concentrations of 50 μM) and a combination of short tubules and hemispherical caps (at concentrations of 200 μM). These large changes in restructuring are generally consistent with the larger changes in frequency and dissipation measured by QCM-D. The increased bilayer reformation observed here could result from complexation of Ca^{2+} to both the DOPS serine head group and the hydrolyzed homoserine head group of 3-oxo-C12-HS, as discussed above.[41]

The introduction of 3-oxo-C12-AHL to DOPS-containing bilayers also led to significant differences in the membrane remodeling observed as compared to single-component DOPC bilayers. As shown in Figure 8(B,D) and Figure S8(C,D) introduction of 3-oxo-C12-AHL at concentrations of both 50 and 200 μM led to the formation of long, extended tubule structures (~100 μm in length) on the surface of the bilayer, many of which did not collapse into hemispherical caps during the time course of these experiments (360 sec). These tubules were much longer than those observed on single-component DOPC bilayers in the presence of Ca^{2+}, consistent with the suggestions of substantially different behaviors in this system that arose in our QCM-D measurements described above (Figures 7 and S7C). We note that 3-oxo-C12-AHL is a non-ionic amphiphile, and thus cannot form ionic complexes with Ca^{2+} in the manner proposed and discussed above for experiments involving anionic 3-oxo-C12-HS. It is possible, however, that the differences in restructuring observed using 3-oxo-C12-AHL could result from calcium-induced clustering of DOPS on the surface of the bilayer,[15,39–41] or from an imbalance of Ca^{2+} on the outer leaflet of the bilayer resulting from a continuous flow of Ca^{2+} across the surface.[15,42] It is well established that the formation of lipid domains (similar to those observed from calcium induced anionic lipid clustering)[76,77] or an imbalance of calcium in the two leaflets of DOPS-containing bilayers[15,42] can result in the formation of bilayer curvature. Either of these effects could, in theory, promote the subsequent formation of high curvature structures (e.g., tubules)

on the surface of a bilayer upon contact with added amphiphiles, consistent with the microscopy results reported here. Overall, the results of these studies demonstrate that both lipid composition and other environmental factors (e.g., the presence of Ca^{2+} in the buffer) can lead to changes in the ways that AHLs and their hydrolysis products interact with lipid bilayers and promote subsequent multi-scale phenomena.

Finally, as part of the studies reported here, we also characterized the interactions of 3-oxo-C12-AHL and 3-oxo-C12-HS with DOPC SLBs containing the cationic lipid DOEPC (Figure 1). While cationic lipids such as DOEPC are not found naturally in the membranes of mammalian cells,[1,2] this broad class of materials is used increasingly for the formulation of lipid-based materials for pharmaceutical applications.[78] To explore the potential interactions of AHLs with DOPC-based, mixed-lipid bilayers containing a cationic lipid, we performed an initial set of experiments using 3-oxo-C12-AHL, 3-oxo-C12-HS, and SLBs comprised of 75 mol% DOPC and 25 mol% DOEPC. We observed remodeling of DOEPC-containing SLBs that was, in general, different from that observed for single-component DOPC SLBs or the anionic DOPS-containing SLBs discussed above. The results of those preliminary studies are included and discussed further in the Supporting Information (Figures S9–11). Although additional experiments will be required to probe and understand the dynamics of these DOEPC-containing membranes more completely, the results of the experiments included here further underscore how changes in the physicochemical properties of lipids and lipid membranes can affect their interactions with AHLs and related derivatives.

Conclusion

We have reported on the influence of membrane composition on multi-scale remodeling that occurs in model mixed-lipid bilayers upon contact with the bacterial quorum sensing signal 3-oxo-C12-AHL and its anionic head group hydrolysis product 3-oxo-C12-HS. As a first step toward understanding the interactions of this important bacterial signal with more complex biological membranes, we investigated interactions of SLBs composed of the phospholipid DOPC either alone or in mixtures containing cholesterol, DOPE, or DOPS using fluorescence microscopy and QCM-D. Overall, we observed these mixed-lipid membranes to undergo remodeling events that differ substantially in the nature, extent, and dynamics of bilayer features that from (e.g., tubules and hemispherical caps of varying morphology) compared to features observed to form in single-component DOPC membranes. We attribute these differences, at least in part, to the influence of lipid structure and membrane composition on the relative timescales of molecular (e.g., AHL or constituent lipid) flip-flop,[21,36] lipid packing defects,[6,37,38] lipid phase segregation,[15,39–41] and the generation of spontaneous curvature[15,42] in these materials and, thus, differences in the ways that these mixed-lipid bilayers regulate or relieve bilayer stresses that can accumulate upon the adsorption and intercalation of 3-oxo-C12-AHL or 3-oxo-C12-HS.

Many common Gram negative bacteria use AHLs to communicate with each other[22–24] and regulate group behaviors such as virulence factor production,[56] swarming,[79] and biofouling,[80] and a growing body of experimental results suggests that AHLs may also interact with the membranes of mammalian cells and play important roles in regulating

host-cell interactions.[29,32] Each of the individual lipids investigated here is representative of classes of lipids that comprise mammalian cell membranes.[2] The two-component, mixed-lipid membranes investigated here lack the full range of compositional and functional complexity typical of biological membranes, but they present useful models to probe and understand the ways that membrane composition can impact interactions with this class of bacterial signals. Mixed-lipid membranes are also useful for the design of many responsive synthetic materials, including vesicle-based vehicles for drug delivery and supported membranes that can serve as components of environmental sensors.[3,4,81] The fundamental studies reported here thus also have the potential to provide guidance for the design of new types of soft materials that can interact with or respond selectively to molecules that bacterial communities use to communicate. Efforts to explore these opportunities are currently underway and will be reported in due course.

Supplementary Material

Refer to Web version on PubMed Central for supplementary material.

Acknowledgements.

Financial support for this work was provided by the National Science Foundation (NSF) through a grant provided to the UW–Madison Materials Research Science and Engineering Center (MRSEC; DMR-1720415). H.E.B. acknowledges support from the National Institutes of Health (R35 GM131817). The authors acknowledge the use of instrumentation supported by the NSF through the UW MRSEC (DMR-1720415). We thank Lawrence M. Chen for many helpful discussions. C. G. G. was supported in part by a NSF Graduate Research Fellowship.

References

1. Spector AA; Yorek MA, Membrane Lipid-Composition And Cellular Function. J. Lipid Res 1985, 26 (9), 1015–1035. [PubMed: 3906008]
2. van Meer G; de Kroon A, Lipid map of the mammalian cell. J. Cell Sci 2011, 124 (1), 5–8. [PubMed: 21172818]
3. Mura S; Nicolas J; Couvreur P, Stimuli-responsive nanocarriers for drug delivery. Nat. Mater 2013, 12 (11), 991–1003. [PubMed: 24150417]
4. Lee Y; Thompson DH, Stimuli-responsive liposomes for drug delivery. Wiley Interdiscip. Rev. Nanomed. Nanobiotechnol 2017, 9 (5), e1450.
5. Casares D; Escriba PV; Rossello CA, Membrane Lipid Composition: Effect on Membrane and Organelle Structure, Function and Compartmentalization and Therapeutic Avenues. Int. J. Mol. Sci 2019, 20 (9), 2167. [PubMed: 31052427]
6. Bigay J; Antonny B, Curvature, Lipid Packing, and Electrostatics of Membrane Organelles: Defining Cellular Territories in Determining Specificity. Dev. Cell 2012, 23 (5), 886–895. [PubMed: 23153485]
7. Dimova R, Recent developments in the field of bending rigidity measurements on membranes. Adv. Colloid Interface Sci 2014, 208, 225–234. [PubMed: 24666592]
8. Subczynski WK; Pasenkiewicz-Gierula M; Widomska J; Mainali L; Raguz M, High Cholesterol/Low Cholesterol: Effects in Biological Membranes: A Review. Cell Biochem. Biophys 2017, 75 (3-4), 369–385. [PubMed: 28417231]
9. Faizi HA; Frey SL; Steinkuhler J; Dimova R; Vlahovska PM, Bending rigidity of charged lipid bilayer membranes. Soft Matter 2019, 15 (29), 6006–6013. [PubMed: 31298256]
10. Chernomordik L; Kozlov MM; Zimmerberg J, Lipids in Biological Membrane-Fusion. J. Membr. Biol 1995, 146 (1), 1–14. [PubMed: 7563032]
11. Storck EM; Ozbalci C; Eggert US, Lipid Cell Biology: A Focus on Lipids in Cell Division. Annu. Rev. Biochem 2018, 87, 839–869. [PubMed: 29494237]

12. Paliwal SR; Paliwal R; Vyas SP, A review of mechanistic insight and application of pH-sensitive liposomes in drug delivery. Drug Delivery 2015, 22 (3), 231–242. [PubMed: 24524308]
13. Binder H; Zschornig O, The effect of metal cations on the phase behavior and hydration characteristics of phospholipid membranes. Chem. Phys. Lipids 2002, 115 (1-2), 39–61. [PubMed: 12047897]
14. Javanainen M; Melcrova A; Magarkar A; Jurkiewicz P; Hof M; Jungwirth P; Martinez-Seara H, Two cations, two mechanisms: interactions of sodium and calcium with zwitterionic lipid membranes. Chem. Commun 2017, 53 (39), 5380–5383.
15. Graber ZT; Shi Z; Baumgart T, Cations induce shape remodeling of negatively charged phospholipid membranes. Phys. Chem. Chem. Phys 2017, 19 (23), 15285–15295. [PubMed: 28569910]
16. Zimmerberg J; Kozlov MM, How proteins produce cellular membrane curvature. Nat. Rev. Mol. Cell Biol 2006, 7 (1), 9–19. [PubMed: 16365634]
17. McMahon HT; Boucrot E, Membrane curvature at a glance. J. Cell Sci 2015, 128 (6), 1065–1070. [PubMed: 25774051]
18. Heerklotz H, Interactions of surfactants with lipid membranes. Q. Rev. Biophys 2008, 41 (3-4), 205–264. [PubMed: 19079805]
19. Yoon BK; Jackman JA; Kim MC; Cho NJ, Spectrum of Membrane Morphological Responses to Antibacterial Fatty Acids and Related Surfactants. Langmuir 2015, 31 (37), 10223–10232. [PubMed: 26325618]
20. Yoon BK; Jackman JA; Park S; Mokrzecka N; Cho NJ, Characterizing the Membrane-Disruptive Behavior of Dodecylglycerol Using Supported Lipid Bilayers. Langmuir 2019, 35 (9), 3568–3575. [PubMed: 30720282]
21. Kawakami LM; Yoon BK; Jackman JA; Knoll W; Weiss PS; Cho NJ, Understanding How Sterols Regulate Membrane Remodeling in Supported Lipid Bilayers. Langmuir 2017, 33 (51), 14756–14765. [PubMed: 29182278]
22. Fuqua C; Greenberg EP, Listening in on bacteria: Acyl-homoserine lactone signalling. Nat. Rev. Mol. Cell Biol 2002, 3 (9), 685–695. [PubMed: 12209128]
23. Waters CM; Bassler BL, Quorum sensing: Cell-to-cell communication in bacteria. Annu. Rev. Cell Dev. Biol 2005, 21, 319–346. [PubMed: 16212498]
24. Papenfort K; Bassler BL, Quorum sensing signal-response systems in Gram-negative bacteria. Nat. Rev. Microbiol 2016, 14 (9), 576–588. [PubMed: 27510864]
25. Gahan CG; Patel SJ; Chen LM; Manson DE; Ehmer ZJ; Blackwell HE; Van Lehn RC; Lynn DM, Bacterial Quorum Sensing Signals Promote Large-Scale Remodeling of Lipid Membranes. Langmuir 2021, 37, 9120–9136. [PubMed: 34283628]
26. Gahan CG; Van Lehn RC; Blackwell HE; Lynn DM, Interactions of Bacterial Quorum Sensing Signals with Model Lipid Membranes: Influence of Acyl Tail Structure on Multiscale Response. Langmuir 2021, 37, 12049–12058. [PubMed: 34606725]
27. Davis BM; Richens JL; O'Shea P, Label-Free Critical Micelle Concentration Determination of Bacterial Quorum Sensing Molecules. Biophys. J 2011, 101 (1), 245–254. [PubMed: 21723835]
28. Gahan CG; Patel SJ; Boursier ME; Nyffeler KE; Jennings J; Abbott NL; Blackwell HE; Van Lehn RC; Lynn DM, Bacterial Quorum Sensing Signals Self-Assemble in Aqueous Media to Form Micelles and Vesicles: An Integrated Experimental and Molecular Dynamics Study. J. Phys. Chem. B 2020, 124 (18), 3616–3628. [PubMed: 32271573]
29. Davis BM; Jensen R; Williams P; O'Shea P, The Interaction of N-Acylhomoserine Lactone Quorum Sensing Signaling Molecules with Biological Membranes: Implications for Inter-Kingdom Signaling. PLoS One 2010, 5 (10), e13522. [PubMed: 20975958]
30. Jakubczyk D; Barth C; Kubas A; Anastassacos F; Koelsch P; Fink K; Schepers U; Brenner-Weiss G; Brase S, Deuterium-labelled N-acyl-l-homoserine lactones (AHLs)-inter-kingdom signalling molecules-synthesis, structural studies, and interactions with model lipid membranes. Anal. Bioanal. Chem 2012, 403 (2), 473–482. [PubMed: 22367286]
31. Barth C; Jakubczyk D; Kubas A; Anastassacos F; Brenner-Weiss G; Fink K; Schepers U; Brase S; Koelsch P, Interkingdom Signaling: Integration, Conformation, and Orientation of N-Acyl-L-

homoserine Lactones in Supported Lipid Bilayers. Langmuir 2012, 28 (22), 8456–8462. [PubMed: 22568488]

32. Song DK; Meng JC; Cheng J; Fan Z; Chen PY; Ruan HF; Tu ZY; Kang N; Li N; Xu Y; Wang XB; Shi F; Mu LB; Li TF; Ren WR; Lin X; Zhu J; Fang XH; Amrein MW; Wu WH; Yan LT; Lu JH; Xia T; Shi Y, *Pseudomonas aeruginosa* quorum-sensing metabolite induces host immune cell death through cell surface lipid domain dissolution. Nat. Microbiol 2019, 4 (1), 97–111. [PubMed: 30510173]
33. Yoon BK; Jackman JA; Kim MC; Sut TN; Cho NJ, Correlating Membrane Morphological Responses with Micellar Aggregation Behavior of Capric Acid and Monocaprin. Langmuir 2017, 33 (11), 2750–2759. [PubMed: 28263610]
34. Glansdorp FG; Thomas GL; Lee JJK; Dutton JM; Salmond GPC; Welch M; Spring DR, Synthesis and stability of small molecule probes for *Pseudomonas aeruginosa* quorum sensing modulation. Org. Biomol. Chem 2004, 2 (22), 3329–3336. [PubMed: 15534711]
35. Boursier ME; Combs JB; Blackwell HE, N-Acyl L-Homocysteine Thiolactones Are Potent and Stable Synthetic Modulators of the RhlR Quorum Sensing Receptor in *Pseudomonas aeruginosa*. ACS Chem. Biol 2019, 14 (2), 186–191. [PubMed: 30668907]
36. Bruckner RJ; Mansy SS; Ricardo A; Mahadevan L; Szostak JW, Flip-Flop-Induced Relaxation of Bending Energy: Implications for Membrane Remodeling. Biophys. J 2009, 97 (12), 3113–3122. [PubMed: 20006948]
37. Brink-van der Laan EV; Killian JA; de Kruijff B, Nonbilayer lipids affect peripheral and integral membrane proteins via changes in the lateral pressure profile. Biochim. Biophys. Acta, Biomembr 2004, 1666 (1-2), 275–288.
38. Anglin TC; Conboy JC, Kinetics and Thermodynamics of Flip-Flop in Binary Phospholipid Membranes Measured by Sum-Frequency Vibrational Spectroscopy. Biochemistry 2009, 48 (43), 10220–10234. [PubMed: 19746969]
39. Ohnishi S; Ito T, Calcium-Induced Phase Separations in Phosphatidylserine-Phosphatidylcholine Membranes. Biochemistry 1974, 13 (5), 881–887. [PubMed: 4360353]
40. Flynn KR; Martin LL; Ackland ML; Torriero AAJ, Real-Time Quartz Crystal Microbalance Monitoring of Free Docosahexaenoic Acid Interactions with Supported Lipid Bilayers. Langmuir 2016, 32 (45), 11717–11727. [PubMed: 27728769]
41. Melcrova A; Pokorna S; Pullanchery S; Kohagen M; Jurkiewicz P; Hof M; Jungwirth P; Cremer PS; Cwiklik L, The complex nature of calcium cation interactions with phospholipid bilayers. Sci. Rep 2016, 6, 38035. [PubMed: 27905555]
42. Doosti BA; Pezeshkian W; Bruhn DS; Ipsen JH; Khandelia H; Jeffries GDM; Lobovidna T, Membrane Tubulation in Lipid Vesicles Triggered by the Local Application of Calcium Ions. Langmuir 2017, 33 (41), 11010–11017. [PubMed: 28910109]
43. Churchward MA; Rogasevskaia T; Brandman DM; Khosravani H; Nava P; Atkinson JK; Coorssen JR, Specific lipids supply critical negative spontaneous curvature - An essential component of native Ca^{2+}-triggered membrane fusion. Biophys. J 2008, 94 (10), 3976–3986. [PubMed: 18227127]
44. Kooijman EE; Chupin V; Fuller NL; Kozlov MM; de Kruijff B; Burger KNJ; Rand PR, Spontaneous curvature of phosphatidic acid and lysophosphatidic acid. Biochemistry 2005, 44 (6), 2097–2102. [PubMed: 15697235]
45. Sut TN; Jackman JA; Cho NJ, Understanding How Membrane Surface Charge Influences Lipid Bicelle Adsorption onto Oxide Surfaces. Langmuir 2019, 35 (25), 8436–8444. [PubMed: 31141663]
46. Sut TN; Park S; Choe Y; Cho NJ, Characterizing the Supported Lipid Membrane Formation from Cholesterol-Rich Bicelles. Langmuir 2019, 35 (47), 15063–15070. [PubMed: 31670521]
47. Kolahdouzan K; Jackman JA; Yoon BK; Kim MC; Johal MS; Cho NJ, Optimizing the Formation of Supported Lipid Bilayers from Bicellar Mixtures. Langmuir 2017, 33 (20), 5052–5064. [PubMed: 28457139]
48. Lichtenberg D; Ahyayauch H; Alonso A; Goni FM, Detergent solubilization of lipid bilayers: A balance of driving forces. Trends Biochem. Sci 2013, 38 (2), 85–93. [PubMed: 23290685]

49. Jackman JA; Cho NJ, Supported Lipid Bilayer Formation: Beyond Vesicle Fusion. Langmuir 2020, 36 (6), 1387–1400. [PubMed: 31990559]
50. Kim MC; Gunnarsson A; Tabaei SR; Hook F; Cho NJ, Supported lipid bilayer repair mediated by AH peptide. Phys. Chem. Chem. Phys 2016, 18 (4), 3040–3047. [PubMed: 26739239]
51. Silvius JR, Thermotropic Phase Transitions of Pure Lipids in Model Membranes and Their Modifications by Membrane Proteins. In Lipid-Protein Interactions, John Wiley & Sons, Inc.: New York, 1982; pp 246–275.
52. Welsh MA; Blackwell HE, Chemical genetics reveals environment-specific roles for quorum sensing circuits in *Pseudomonas aeruginosa*. Cell Chem. Biol 2016, 23, 361–369. [PubMed: 26905657]
53. Fuqua C; Parsek MR; Greenberg EP, Regulation of gene expression by cell-to-cell communication: Acyl-homoserine lactone quorum sensing. Annu. Rev. Genet 2001, 35, 439–468. [PubMed: 11700290]
54. Jensen PO; Givskov M; Bjarnsholt T; Moser C, The immune system vs. *Pseudomonas aeruginosa* biofilms. FEMS Immunol. Med. Microbiol 2010, 59 (3), 292–305. [PubMed: 20579098]
55. Reis RS; Pereira AG; Neves BC; Freire DMG, Gene regulation of rhamnolipid production in *Pseudomonas aeruginosa* - A review. Bioresour. Technol 2011, 102 (11), 6377–6384. [PubMed: 21498076]
56. Rutherford ST; Bassler BL, Bacterial quorum sensing: its role in virulence and possibilities for its control. Cold Spring Harbor perspectives in medicine 2012, 2 (11), a012427. [PubMed: 23125205]
57. de Abreu PM; Farias PG; Paiva GS; Almeida AM; Morais PV, Persistence of microbial communities including *Pseudomonas aeruginosa* in a hospital environment: a potential health hazard. BMC Microbiol. 2014, 14, 118. [PubMed: 24885173]
58. Richter RP; Brisson AR, Following the formation of supported lipid bilayers on mica: A study combining AFM, QCM-D, and ellipsometry. Biophys. J 2005, 88 (5), 3422–3433. [PubMed: 15731391]
59. Pedersen UR; Leidy C; Westh P; Peters GH, The effect of calcium on the properties of charged phospholipid bilayers. Biochim. Biophys. Acta, Biomembr 2006, 1758 (5), 573–582.
60. Filippov A; Oradd G; Lindblom G, Effect of NaCl and $CaCl_2$ on the lateral diffusion of zwitterionic and anionic lipids in bilayers. Chem. Phys. Lipids 2009, 159 (2), 81–87. [PubMed: 19477314]
61. Dluhy RA; Cameron DG; Mantsch HH; Mendelsohn R, Fourier-Transform Infrared Spectroscopic Studies of the Effect of Calcium-Ions on Phosphatidylserine. Biochemistry 1983, 22 (26), 6318–6325.
62. Sinn CG; Antonietti M; Dimova R, Binding of calcium to phosphatidylcholine-phosphatidylserine membranes. Colloids Surf., A 2006, 282, 410–419.
63. Charlton TS; de Nys R; Netting A; Kumar N; Hentzer M; Givskov M; Kjelleberg S, A novel and sensitive method for the quantification of N-3-oxoacyl homoserine lactones using gas chromatography-mass spectrometry: Application to a model bacterial biofilm. Environ. Microbiol 2000, 2 (5), 530–541. [PubMed: 11233161]
64. Ortiz BJ; Boursier ME; Barrett KL; Manson DE; Amador-Noguez D; Abbott NL; Blackwell HE; Lynn DM, Liquid Crystal Emulsions That Intercept and Report on Bacterial Quorum Sensing. ACS Appl. Mater. Interfaces 2020, 12 (26), 29056–29065. [PubMed: 32484648]
65. Bennett WFD; MacCallum JL; Hinner MJ; Marrink SJ; Tieleman DP, Molecular View of Cholesterol Flip-Flop and Chemical Potential in Different Membrane Environments. J. Am. Chem. Soc 2009, 131 (35), 12714–12720. [PubMed: 19673519]
66. Yoon BK; Park S; Ma GJ; Kolahdouzan K; Zhdanov VP; Jackman JA; Cho NJ, Competing Interactions of Fatty Acids and Monoglycerides Trigger Synergistic Phospholipid Membrane Remodeling. J. Phys. Chem. Lett 2020, 11 (13), 4951–4957. [PubMed: 32478524]
67. Apel-Paz M; Doncel GF; Vanderlick TK, Impact of membrane cholesterol content on the resistance of vesicles to surfactant attack. Langmuir 2005, 21 (22), 9843–9849. [PubMed: 16229500]
68. Heerklotz H; Seelig J, Leakage and lysis of lipid membranes induced by the lipopeptide surfactin. Eur. Biophys. J 2007, 36 (4-5), 305–314. [PubMed: 17051366]

69. Heerklotz H, Membrane stress and permeabilization induced by asymmetric incorporation of compounds. Biophys. J 2001, 81 (1), 184–195. [PubMed: 11423405]

70. Staykova M; Arroyo M; Rahimi M; Stone HA, Confined Bilayers Passively Regulate Shape and Stress. Phys. Rev. Lett 2013, 110 (2), 028101. [PubMed: 23383939]

71. Vanni S; Hirose H; Barelli H; Antonny B; Gautier R, A sub-nanometre view of how membrane curvature and composition modulate lipid packing and protein recruitment. Nat. Comm 2014, 5 (Art. No. 4916).

72. Allhusen JS; Conboy JC, The Ins and Outs of Lipid Flip-Flop. Acc. Chem. Res 2017, 50 (1), 58–65. [PubMed: 27959517]

73. Pabst G; Hodzic A; Strancar J; Danner S; Rappolt M; Laggner P, Rigidification of neutral lipid bilayers in the presence of salts. Biophys. J 2007, 93 (8), 2688–2696. [PubMed: 17586572]

74. Kucerka N; Ermakova E; Dushanov E; Kholmurodov KT; Kurakin S; Zelinska K; Uhrikova D, Cation-Zwitterionic Lipid Interactions Are Affected by the Lateral Area per Lipid. Langmuir 2021, 37 (1), 278–288. [PubMed: 33356308]

75. Kagawa R; Hirano Y; Taiji M; Yasuoka K; Yasui M, Dynamic interactions of cations, water and lipids and influence on membrane fluidity. J. Membr. Sci 2013, 435, 130–136.

76. Julicher F; Lipowsky R, Domain-Induced Budding of Vesicles. Phys. Rev. Lett 1993, 70 (19), 2964–2967. [PubMed: 10053698]

77. Baumgart T; Hess ST; Webb WW, Imaging coexisting fluid domains in biomembrane models coupling curvature and line tension. Nature 2003, 425 (6960), 821–824. [PubMed: 14574408]

78. Zuhorn IS; Engberts J; Hoekstra D, Gene delivery by cationic lipid vectors: overcoming cellular barriers. Eur. Biophys. J 2007, 36 (4-5), 349–362. [PubMed: 17019592]

79. Daniels R; Reynaert S; Hoekstra H; Verreth C; Janssens J; Braeken K; Fauvart M; Beullens S; Heusdens C; Lambrichts I; De Vos DE; Vanderleyden J; Vermant J; Michiels J, Quorum signal molecules as biosurfactants affecting swarming in Rhizobium etli. Proceedings of the National Academy of Sciences of the United States of America 2006, 103 (40), 14965–14970. [PubMed: 16990436]

80. Davies DG; Parsek MR; Pearson JP; Iglewski BH; Costerton JW; Greenberg EP, The involvement of cell-to-cell signals in the development of a bacterial biofilm. Science 1998, 280 (5361), 295–298. [PubMed: 9535661]

81. Zhou J; Loftus AL; Mulley G; Jenkins ATA, A Thin Film Detection/Response System for Pathogenic Bacteria. J. Am. Chem. Soc 2010, 132 (18), 6566–6570. [PubMed: 20405918]

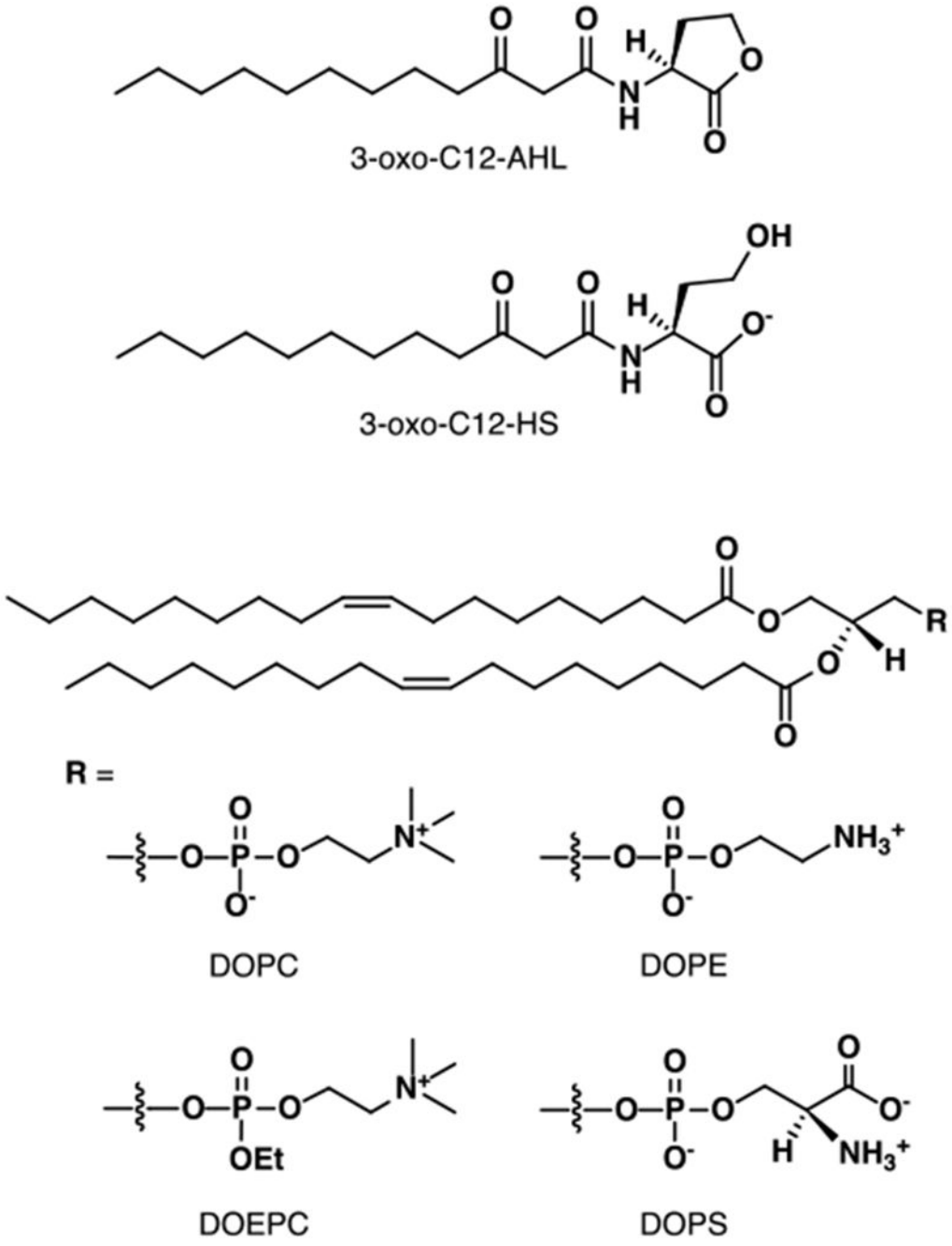

Figure 1:
Structures of the AHL, AHL hydrolysis product, and lipids used in this study. All lipids possessed the same tail structure and varied only in the head group, as indicated by the four R groups shown.

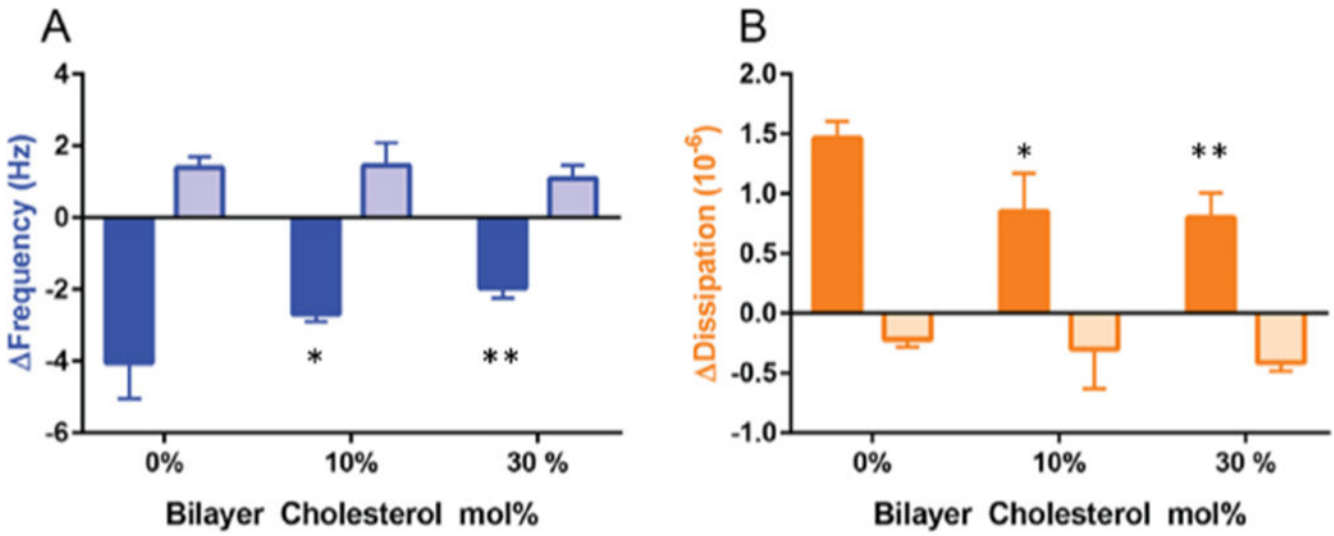

Figure 2:

Changes in (A) frequency and (B) dissipation for SLBs with varying cholesterol compositions upon exposure to solutions of 50 μM 3-oxo-C12-AHL for 45 minutes (filled bars) or after 45 minutes of buffer wash (open bars; for the 0% cholesterol bilayers, changes in frequency and dissipation upon washing shown are at 32 minutes, see Supporting Information). The values shown are the means and a single standard deviation of three or four experiments (n = 3–4). Statistical significance compared to 0% cholesterol bilayers is indicated with the following p values: *$p < 0.05$, **$p < 0.01$.

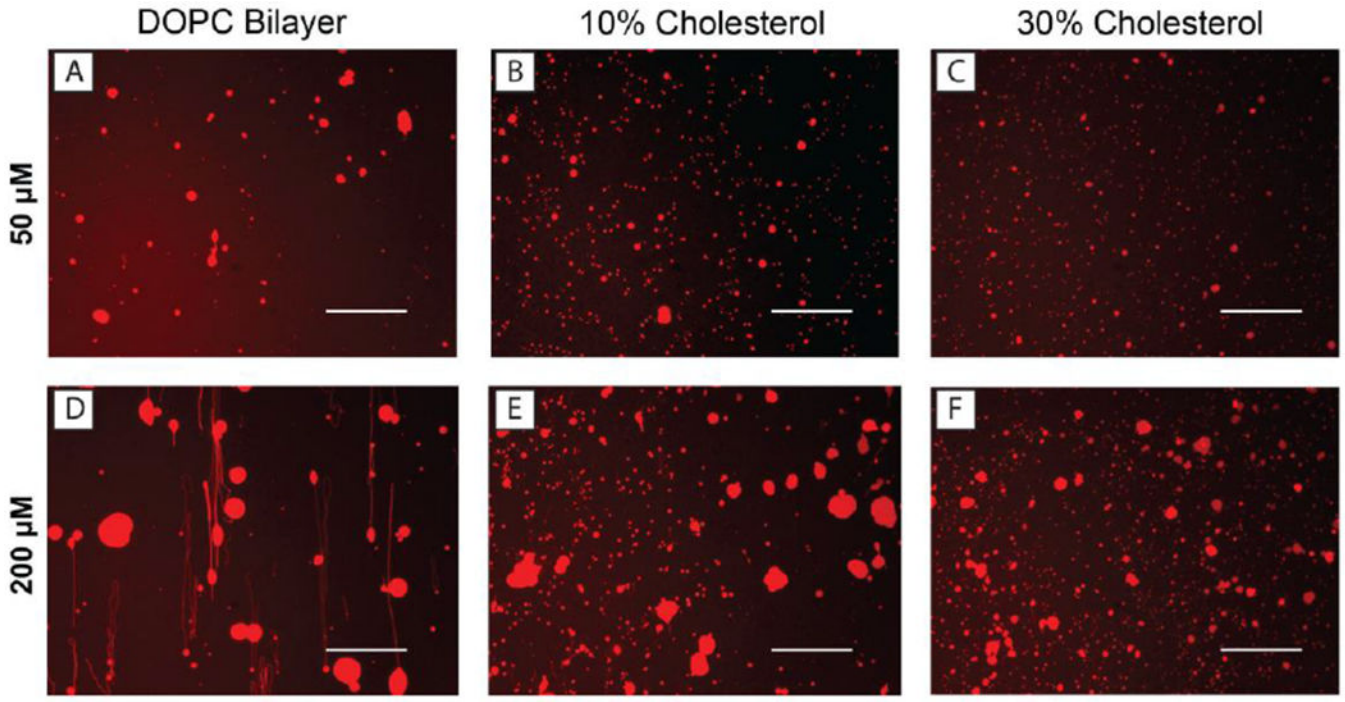

Figure 3:

Representative top-down fluorescence micrographs of fluorescently labeled (A,D) DOPC, (B,E) 10% cholesterol or (C,F) 30% cholesterol SLBs after exposure to a continuous flow of (A-C) 50 μM or (D-F) 200 μM 3-oxo-C12-AHL. Images were acquired 360 seconds after the onset of membrane restructuring. The direction of flow in all images was from the bottom to the top of the image. Scale bars are 30 μm.

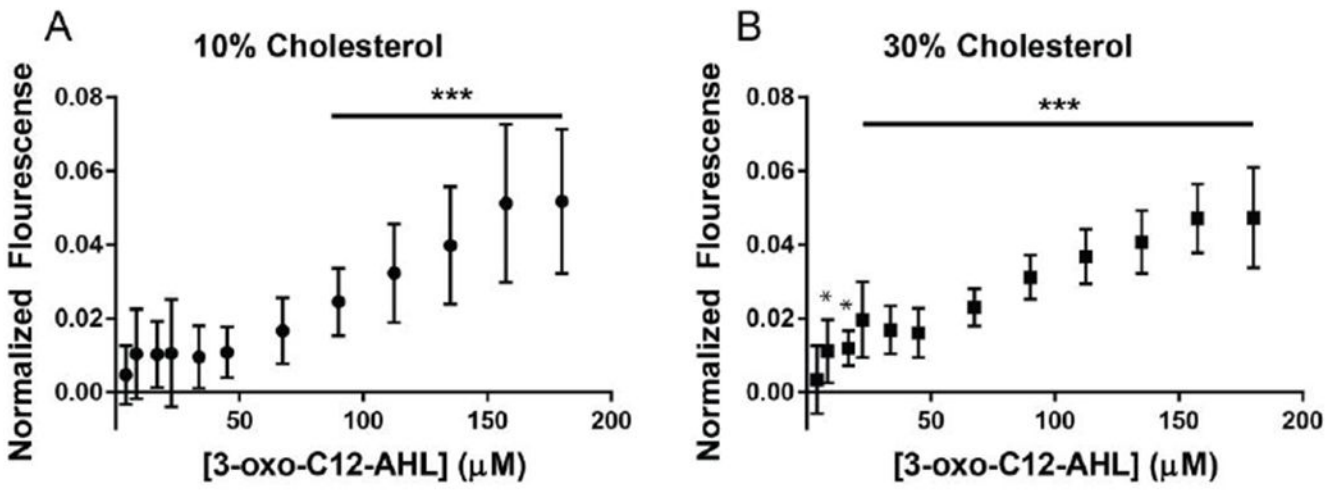

Figure 4:

Normalized calcein fluorescence intensity values in a solution containing 100 μM of calcein-loaded DOPC vesicles containing either (A) 10% cholesterol or (B) 30% cholesterol after exposure to solutions of 3-oxo-C12-AHL at various concentrations. Statistical significance compared to a buffer control is indicated for concentrations with the following p values: *$p < 0.05$, ***$p < 0.001$. All points shown are the average and standard deviation of three independent experiments.

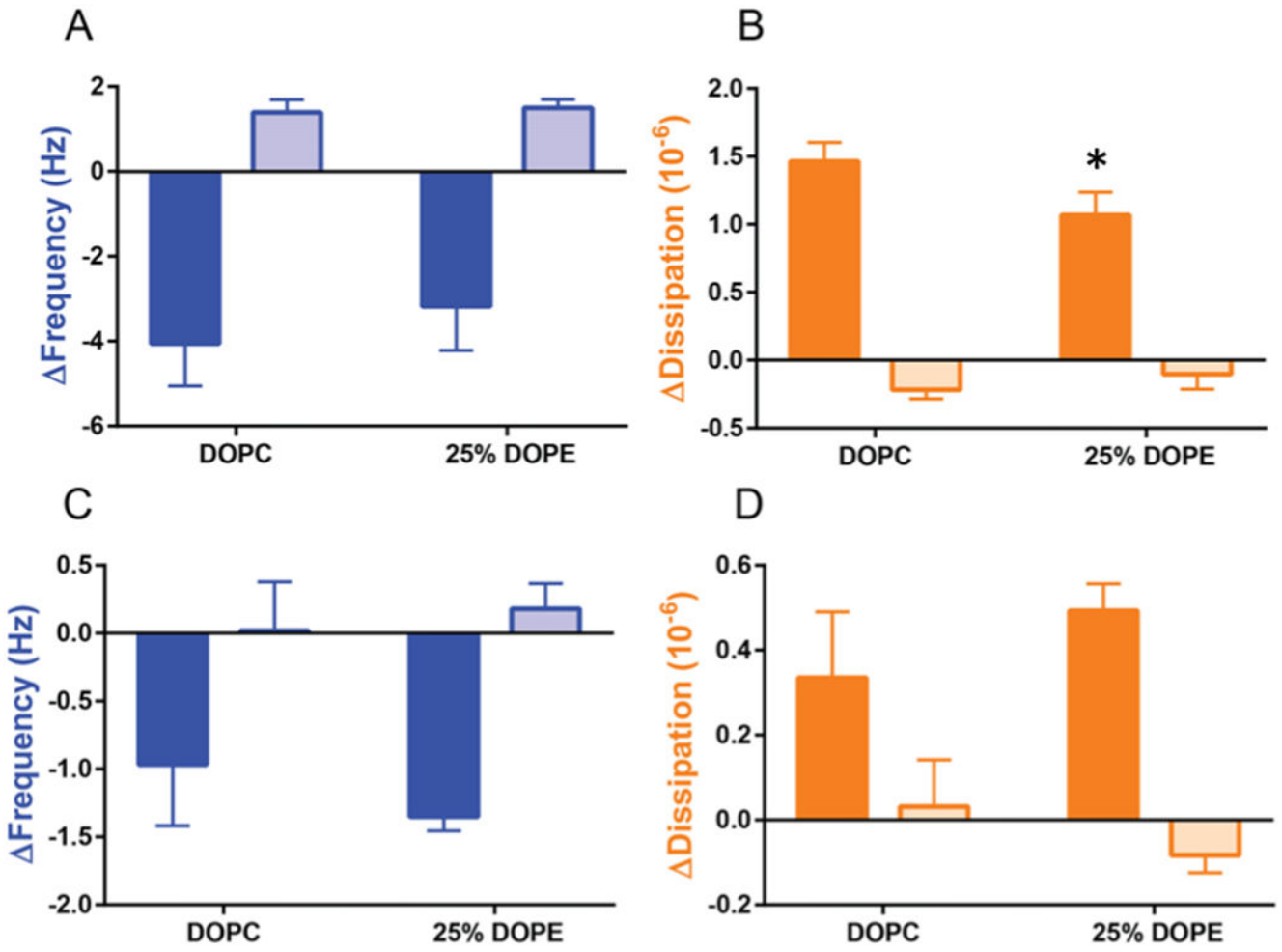

Figure 5:

Changes in (A,C) frequency and (B,D) dissipation for SLBs composed of either 100% DOPC or 75% DOPC/25% DOPE after introducing 50 μM solutions of (A,B) 3-oxo-C12-AHL or (C,D) 3-oxo-C12-HS for 45 minutes (filled bars) or after 45 minutes of buffer wash (open bars; for the DOPC bilayers, changes in frequency and dissipation upon washing are shown at 32 minutes, see Supporting Information). The values shown are the means and a single standard deviation of three or four experiments (n = 3-4). Statistical significance compared to DOPC bilayers upon compound introduction is indicated with the following p values: *$p < 0.05$.

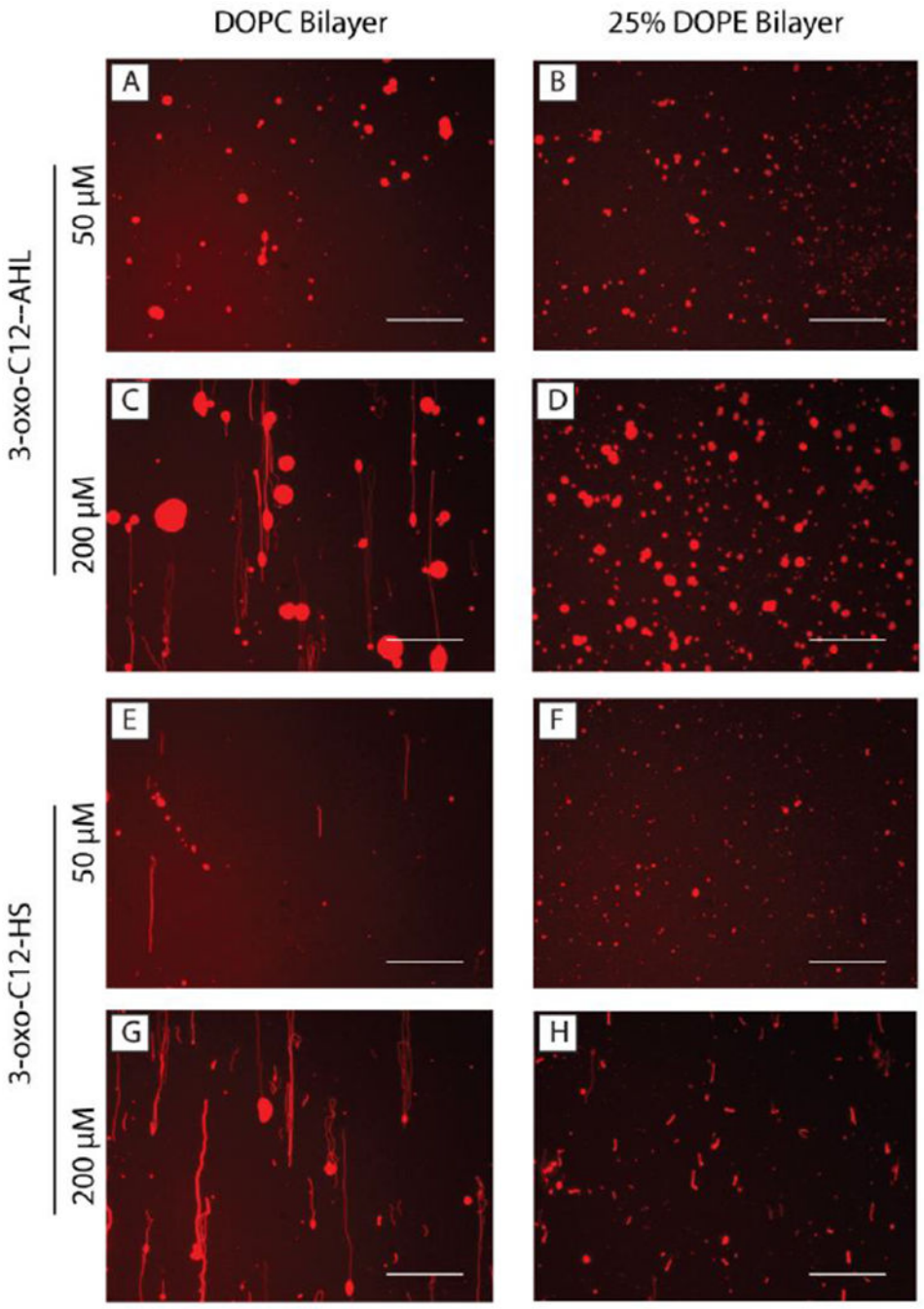

Figure 6:

Representative top-down fluorescence micrographs of fluorescently labeled (A,C,E,G) DOPC or (B,D,F,H) 75% DOPC/25% DOPE SLBs after exposure to a continuous flow of (A,B,E,F) 50 μM or (C,D,G,H) 200 μM solutions of (A-D) 3-oxo-C12-AHL or (E-H) 3-oxo-C12-HS. Images were acquired 360 seconds after the onset of membrane restructuring. The direction of flow in all images was from the bottom to the top of the image. Scale bars are 30 μm.

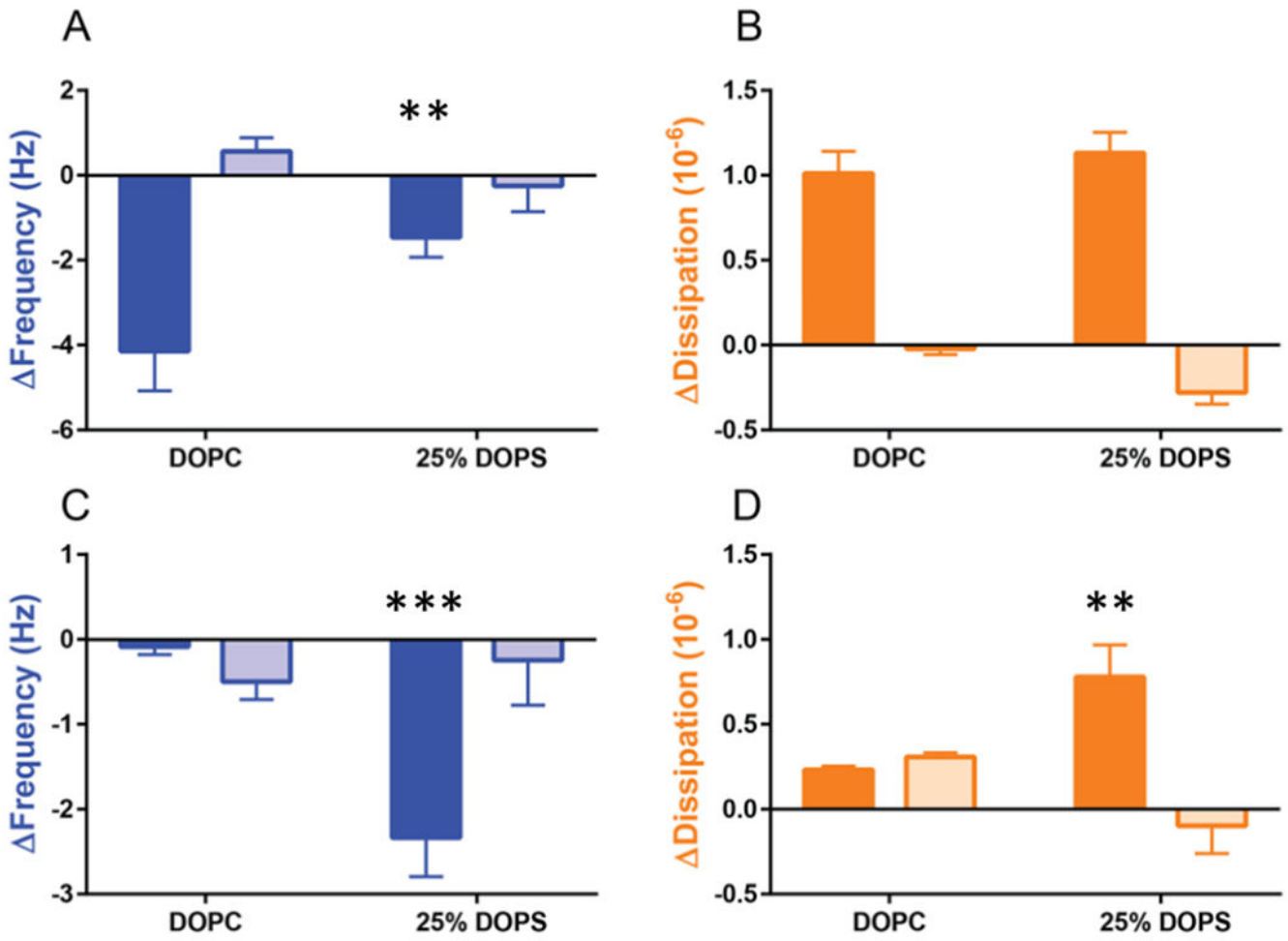

Figure 7:

Changes in (A,C) frequency and (B,D) dissipation for SLBs composed of either DOPC or 75% DOPC/25% DOPS in buffer containing 2 mM $CaCl_2$ after introducing 50 μM solutions of (A,B) 3-oxo-C12-AHL or (C,D) 3-oxo-C12-HS for 45 minutes (filled bars) or after 45 minutes of buffer wash (open bars). Statistical significance compared to DOPC bilayers in buffer containing 2 mM $CaCl_2$ upon compound introduction is indicated with the following p values: **p<0.01, ***p < 0.001. The values shown are the means and a single standard deviation of three or four experiments (n = 3–4).

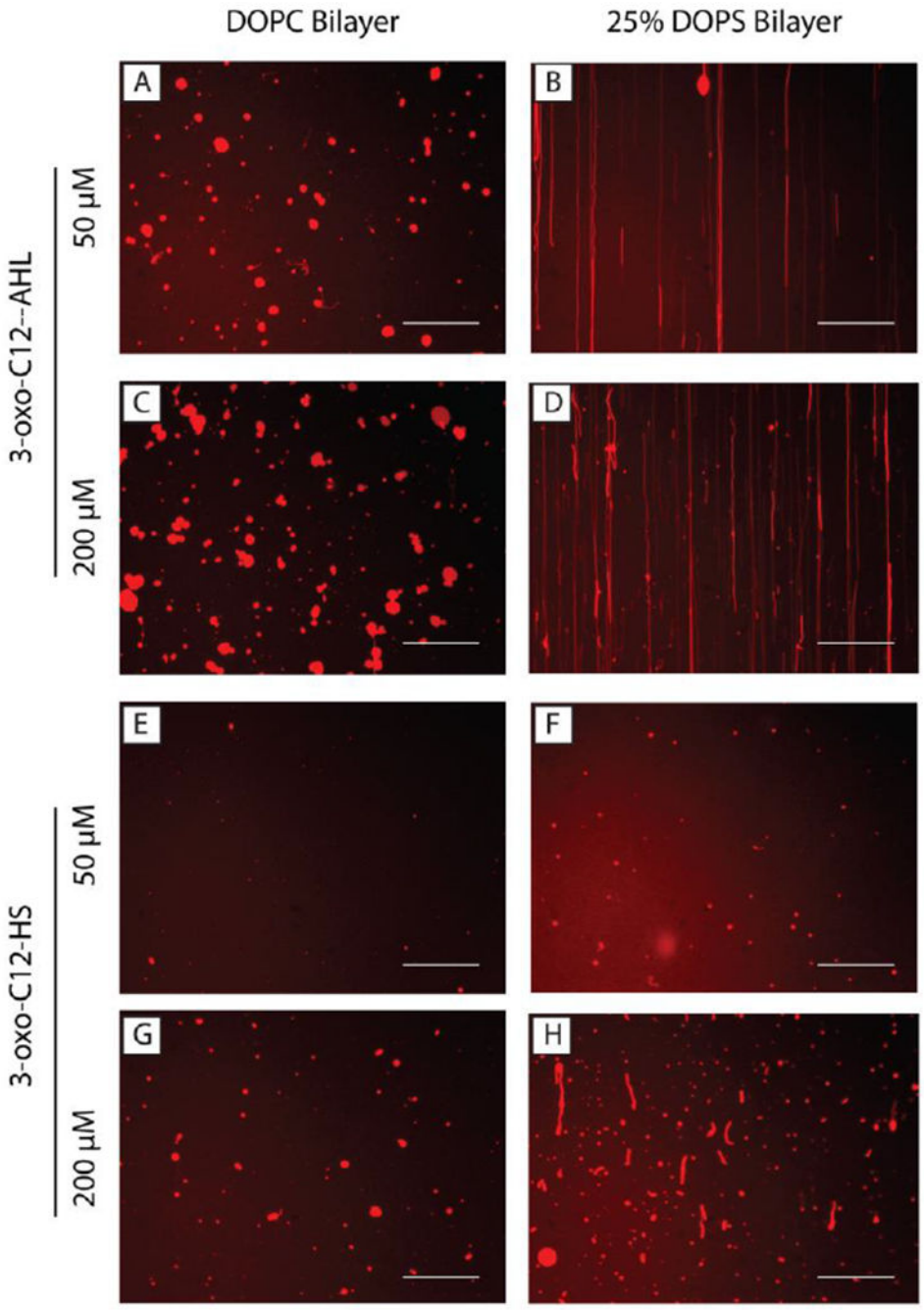

Figure 8:

Representative top-down fluorescence micrographs of fluorescently labeled (A,C,E,G) DOPC or (B,D,F,H) 75% DOPC/25% DOPS SLBs after exposure to a continuous flow of (A,B,E,F) 50 μM or (C,D,G,H) 200 μM solutions (A-D) 3-oxo-C12-AHL or (E-H) 3-oxo-C12-HS in buffer containing $CaCl_2$. Images were acquired 360 seconds after the onset of membrane restructuring. The direction of flow in all images was from the bottom to the top of the image. Scale bars are 30 μm.